



Effect of potassium addition on bimetallic PtSn supported $\theta\text{-Al}_2\text{O}_3$ catalyst for *n*-butane dehydrogenation to olefins



Bhari Mallanna Nagaraja^a, Heon Jung^{a,b}, Dae Ryook Yang^b, Kwang-Deog Jung^{a,*}

^a Clean Energy Research Centre, Korea Institute of Science and Technology, P.O. Box 131 Cheongryang, Seoul 136-791, Republic of Korea

^b Department of Chemical & Biological Engineering, Korea University, Anam-dong, Seongbuk-gu, Seoul 136-701, Republic of Korea

ARTICLE INFO

Article history:

Received 5 July 2013

Received in revised form 15 October 2013

Accepted 27 October 2013

Available online 4 December 2013

Keywords:

n-Butane dehydrogenation

n-Butenes

KPtSn/ $\theta\text{-Al}_2\text{O}_3$ catalyst

Effect of alkali metal

PtSn alloy formation.

ABSTRACT

PtSn/ $\theta\text{-Al}_2\text{O}_3$ catalysts with different amount of potassium (0.4, 0.7, 0.95, 1.2 and 1.45 wt.%) were prepared by an impregnation method, and their catalytic activity in *n*-butane dehydrogenation was investigated at 823 K, an atmospheric pressure and a GHSV of 18,000 mL(g_{cat} h)⁻¹. The compositions listed in order of *n*-C₄⁼ yields at 823 K were as follows: K_{0.95}(PtSn)_{1.5} > (PtSn)_{1.5} > K_{0.4}(PtSn)_{1.5} > K_{0.7}(PtSn)_{1.5} > K_{1.2}(PtSn)_{1.5} > K_{1.45}(PtSn)_{1.5} > K_{0.9}(Pt)_{1.5}. The K_{0.9}(Pt)_{1.5} and K_{0.95}(Sn)_{1.5} catalyst severely deactivated in *n*-butane dehydrogenation. The (PtSn)_{1.5} (without K) catalyst showed the highest *n*-butane conversion, while K_{0.95}(PtSn)_{1.5} did the highest *n*-C₄⁼ yield. The small amount of potassium on bimetallic PtSn/ $\theta\text{-Al}_2\text{O}_3$ catalyst improved *n*-C₄⁼ selectivity, but slightly decreased *n*-butane conversion, resulting in the increase of *n*-C₄⁼ yield. The effect of potassium was caused by blocking the acid sites of Pt catalyst. The TPR and HAADF STEM-EDS study suggested the reduction procedure of the Pt, Sn and K species. However, the higher loaded potassium (1.2 and 1.45 wt.%) doped (PtSn)_{1.5} catalysts were rather highly deactivated because the sizes of Pt particles were increased by weakening the interaction between Pt and Sn. The *n*-C₄⁼ selectivity of the (PtSn)_{1.5} catalyst increased with respect to the reaction, while that of the potassium doped catalysts maintained the high *n*-C₄⁼ selectivity from the beginning of the reaction. Also, different alkali metals (Ca, Na and Li) were tested for the comparison with K. The potassium doped catalyst showed the highest *n*-C₄⁼ yield among the other alkali metals for *n*-butane dehydrogenation.

© 2013 Elsevier B.V. All rights reserved.

1. Introduction

The dehydrogenation of butane (*n*- and iso) into olefins is a significant process used for the industrial application such as plastics, synthetic rubbers, automotive fuel components, and petrochemical products [1–4]. Butenes are used for the production of methyl tertiary butyl ether and methacrylates as an additive to gasoline to improve the octane number [5]. In particular, *n*-butenes from the dehydrogenation of butane can be used as a feedstock for the production of 1,4-butadiene. Many authors reported on PtSn catalysts with various supports [3,4,6–9] and alkali promoted (K, Li, Mg, and La) [5,10–18] PtSn catalysts for isobutane dehydrogenation reaction. Llorca et al. reported the magnesia supported PtSn catalysts with different Pt content for isobutane dehydrogenation reaction. The conversion and selectivity of Pt catalyst was increased with the addition of Sn, which was explained by the dilution and electron effect on Pt by Sn [9]. Cortright and Dumesic reported that the addition of potassium to Pt/Sn/SiO₂ increased the selectivity

for isobutane dehydrogenation by reducing the size of surface Pt ensembles [10]. Siri et al. studied the modifying effects of alkaline metals on the acid properties of the support and on the behavior of PtSn/ $\gamma\text{-Al}_2\text{O}_3$ catalytic systems for isobutane dehydrogenation [11]. They reported that the isopropyl alcohol transformation rate decreased drastically with the addition of alkaline metals according to the sequence of Li < Na < K. The addition of K improved the selectivity to butenes as well as the stability of the catalyst. Zhang et al. observed that the suitable addition of potassium and tin resulted in an increase in the platinum dispersion and a decrease in the catalyst acidity, which was due to the synergistic effect between potassium and tin [12]. The synergistic effect could prevent coke formation that covered the active metal and facilitate the transfer of the deposited carbon from the metal to the support. Tasbihi et al. reported the effect of potassium and lithium addition on catalytic performance of Pt–Sn/Al₂O₃ catalyst for isobutane dehydrogenation [14]. The potassium doped catalyst showed better activity as compared with lithium one, which was mainly related to their structural characteristics and electronic properties. The improved selectivity to isobutene was suggested by reducing acidity of the support. Rodriguez et al. reported that the incorporation of Sn and Li also improved the activity and selectivity for light-paraffin

* Corresponding author. Tel.: +82 2 9585218; fax: +82 2 9585219.

E-mail address: jkdcat@kist.re.kr (K.-D. Jung).

dehydrogenation by inhibiting isomerization and cracking reaction [15]. Zhang and co-workers reported that the presence of Mg or La in the PtSnK/Al₂O₃ catalysts increased the activity and selectivity of butenes for isobutane dehydrogenation reaction [17,18]. The addition of Mg or La stabilized the oxidation states of Sn species, increasing the platinum dispersion and decreasing carbon deposition. The addition of alkali metals to oxide catalysts has been found to increase selectivity to olefins in isobutane dehydrogenation reactions. The alkali metals such as Li, Na and K could improve the catalytic activity, selectivity and stability for isobutene dehydrogenation [11,12]. The important phenomenon was attributed to a geometric modification of the metallic phase by the alkali metals, which could effectively inhibited the acidity on the supports [11,14,19,20].

A few researchers have studied *n*-butane dehydrogenation reaction using PtSn catalyst with different supports [21–25]. Bocanegra et al. reported bimetallic PtSn and trimetallic InPtSn catalysts with different supports (γ -Al₂O₃, ZnAl₂O₄ and MgAl₂O₄) for *n*-butane dehydrogenation. The addition of In and/or Sn on Pt sites induced geometric effects resulted from a dilution of the Pt surface, leading to the formation of alloys and/or intermetallic compounds to increase the catalytic activity [21–23]. Ballarini et al. have studied on the *n*-butane dehydrogenation reaction with PtSn and PtGe supported on γ -Al₂O₃ deposited on sphere shaped α -Al₂O₃ by a wash coating method [22,23]. In their report, it was observed that the catalytic activity was improved by the addition of Sn on 0.5Pt and Ge on γ -Al₂O₃/ α -Al₂O₃ support. The increases of the catalytic activity mainly depended on the composition of Sn and Pt, which exhibited low electronic interaction in probable alloys [24,25].

Recently, we studied the selective and stable bimetallic (PtSn)_{x,x} and Pt_{1.5}Sn_{x,x} supported θ -Al₂O₃ catalysts for dehydrogenation of *n*-butane to *n*-butenes [26]. 1.5 wt.% (PtSn)/ θ -Al₂O₃ catalyst showed highest *n*-C₄⁺ yield and the catalyst was stable among the other samples for *n*-butane dehydrogenation reaction. So far, there were little reports on potassium doped PtSn/ θ -Al₂O₃ catalyst for *n*-butane dehydrogenation reaction. In the present work, the different wt.% of potassium doped on 1.5 wt.% (PtSn)/ θ -Al₂O₃ catalysts were studied for *n*-butane dehydrogenation reaction. The 0.95 wt.% K doped catalyst showed maximum *n*-C₄⁺ yield among the other potassium loaded samples. XRD patterns and TEM images confirmed the presence of PtSn alloy on the prepared bimetallic PtSn catalysts. The Pt, Sn and K particles were clearly observed at the same position, which was confirmed by HAADF STEM and corresponding EDS mapping. The *n*-butane dehydrogenation was conducted at different temperatures (773–873 K), and the activity of the catalysts was explained by the characteristics of the catalysts in CO chemisorption, XRD and TPR analysis. We were also studied on the different alkali metals (K, Ca, Na and Li) doped (PtSn)_{1.5}/ θ -Al₂O₃ catalyst for *n*-butane dehydrogenation reaction. The potassium doped catalyst showed the better *n*-C₄⁺ yield and *n*-C₄⁺ selectivity among the other catalysts.

2. Experimental

2.1. Preparation of the catalyst

The equal weight percentage of Pt and Sn (1.5 wt.%) was supported on θ -Al₂O₃ by co-impregnation method, using hydrogen hexachloroplatinate(IV) hydrate (H₂PtCl₆·nH₂O, n = 5.8, Kojima Chemicals Co., Ltd., Japan, purity = 99%) and tin(II) chloride dihydrate (SnCl₂·2H₂O, Sigma-Aldrich, St. Louis, USA, purity = 98%) salt as precursors. Weighed amount of Pt and Sn salt was placed in a 50 ml beaker and dissolved in a required quantity of ethanol. Sphere-shaped θ -Al₂O₃ support (~3 mm) was prepared by calcining the spherical γ -Al₂O₃ at 1273 K for 6 h (γ -Al₂O₃ support was

supplied by Hyosung Company, South Korea). The θ -Al₂O₃ support was added into the beaker with Pt and Sn solution. Ethanol was removed by evaporation on a hot plate, and the residue was dried at 393 K overnight and calcined at 773 K for 4 h in air. The calcined θ -alumina supported PtSn catalyst was designated as (PtSn)_{1.5}.

Samples of the support material containing different amounts of potassium were prepared by adding the appropriate quantities of aqueous solutions of potassium hydroxide (Fluka, Purity = ≥ 86%) to (PtSn)_{1.5}, so that the final resultant materials contained 0.4, 0.7, 0.95 1.2 and 1.45 wt.% of K; after drying the samples at 393 K overnight the catalysts were calcined in air at 773 K for 4 h. The samples were designated as K_{0.4}(PtSn)_{1.5}, K_{0.7}(PtSn)_{1.5}, K_{0.95}(PtSn)_{1.5}, K_{1.2}(PtSn)_{1.5} and K_{1.45}(PtSn)_{1.5} and mono metallic catalysts were designated as K_{0.9}(Pt)_{1.5} and K_{0.95}(Sn)_{1.5}. The potassium, Pt and Sn contents of the samples (Table 1) were determined by an atomic absorption spectroscopy. The other alkali metals such as 1.0 wt.% Na, Ca and Li supported (PtSn)_{1.5} catalysts were also prepared by an impregnation method. The samples were designated as Ca_{0.95}(PtSn)_{1.5}, Na_{0.95}(PtSn)_{1.5} and Li_{0.95}(PtSn)_{1.5}. NaOH (Junsei Chemicals, Co. Ltd., Purity: 97%), Ca(NO₃)₂·4H₂O (Kanto chemicals Co. Inc., Purity: 98.5%) and LiNO₃ (Junsei Chemicals, Co. Ltd., Purity: 98%) were used for the impregnation.

2.2. Characterizations of catalysts

The XRD patterns of the prepared PtSn/ θ -Al₂O₃ catalysts were recorded on a diffractometer (M/S, Shimadzu Instruments, Japan) with Ni-filtered CuK_α (λ = 1.5418 Å) as a radiation source. The operating voltage was 40 kV and the current was 30 mA with a scanning rate of 2θ was 2° min⁻¹. The BET surface areas and N₂ adsorption-desorption measurements were performed at 77 K using an automated gas sorption system (Belsorp II mini, BEL Japan, Inc.). The Barrett-Joyner-Halanda (BJH) method was used for the pore size distribution. The TPR experiments were carried out using a temperature program analyzer (BELCAT, BEL Japan, Inc.).

The NH₃-TPD was performed to determine the acidic properties of the catalysts; the 0.1 g of calcined sample was loaded into a U-tube quartz reactor. Prior to the NH₃ adsorption, the sample was pre-treated at 773 K for 1 h with the flow of helium (30 mL min⁻¹) in order to remove the moisture, physically adsorbed water and other impurities. The sample was cooled down to 373 K in a stream of helium. After cooling, the ammonia (5%NH₃/He, flow: 30 mL min⁻¹) was introduced into the reactor for 1 h. The weakly adsorbed ammonia was removed at 373 K for 1 h. Then, the temperature was ramped from 373 to 1073 K with a heating rate of 10 K min⁻¹ under the flow of helium (30 mL min⁻¹). The NH₃ desorption profile was exhibited in a thermal conductivity detector.

For TPR studies, 0.1 g of a calcined sample was placed between quartz wool in a U-type quartz reactor. The sample was thermally treated under an Ar stream at 673 K for 2 h to remove physically adsorbed water and other impurities. The catalysts were cooled down to the room temperature under pure Ar gas. After the pre-treatment, the catalysts were heated at 10 K min⁻¹ from room temperature up to 1073 K in 5% H₂/Ar stream with a flow rate of 30 mL min⁻¹. The chemisorptions of CO were performed with a pulse chemisorption mode (BELCAT, BEL Japan, Inc.). Prior to measurements, 0.050 g of a sample was thermally treated under a He stream at 773 K for 50 min to remove physically adsorbed water and other impurities. The sample was cooled down to room temperature and heated to 823 K with a heating rate of 10 K min⁻¹ using pure H₂ at a flow rate of 50 mL min⁻¹. The sample was then reduced in a pure H₂ flow at 823 K for 2 h. After the reduction at 823 K, the sample was purged with He gas at the same temperature for 1 h. After cooling to 323 K, the 10% CO/He gas was introduced for the CO chemisorption. CO loop gas was used for each pulse, and

Table 1

Physicochemical properties of mono and bimetallic 1.5 wt.% (PtSn)/ θ -Al₂O₃ catalysts with different potassium loadings.

Catalysts	From ICP (wt.%)			BET surface area (m ² g ⁻¹)			Pore volume of calcined catalysts (cm ³ g ⁻¹)	Average pore diameter of calcined catalysts (nm)
	Pt	Sn	K	Calcined	Reduced	Used		
(PtSn) _{1.5}	1.3	1.35	—	86	82	84	0.327	15.1
K _{0.4} (PtSn) _{1.5}	1.3	1.35	0.40	81	79	78	0.302	15.3
K _{0.7} (PtSn) _{1.5}	1.3	1.35	0.70	80	78	76	0.301	15.3
K _{0.95} (PtSn) _{1.5}	1.3	1.35	0.95	80	79	78	0.303	15.3
K _{1.2} (PtSn) _{1.5}	1.3	1.35	1.2	81	79	81	0.298	14.6
K _{1.45} (PtSn) _{1.5}	1.3	1.35	1.45	81	78	76	0.297	14.7
K _{0.9} (Pt) _{1.5}	1.35	—	0.90	84	84	84	0.326	15.6
K _{0.95} (Sn) _{1.5}	—	1.35	0.95	83	82	80	0.323	15.5

the pulse injections were repeated until saturation. The amount of CO was measured using a thermal conductivity detector. The Pt dispersion of each catalyst was then calculated from the amount of CO adsorbed, taking the stoichiometry factor (SF) as one for CO/Pt_{atm}:

$$\text{Dispersion (\%)} = 100 \times V_s \times SF \times MW / (SW \times F_n \times 22414)$$

where V_s is the cumulative volume of adsorbed CO (cm³ at STP), MW is the molecular weight of Pt metal (g mol⁻¹), SW is the weight of sample and F_n is the Pt fraction in relation to the total catalyst sample weight.

Transmission electron microscopy (TEM) is a technique to calculate the Pt particle size by using CM30 microscope (Philips) with accelerating voltage 50–300 kV using LaB6 source. The high resolution TEM images of the Pt and Sn nanoparticles were characterized by using FEI (Technai F20 G², The Netherland) microscopy working in a STEM mode (Accelerating voltage: 50–200 kV, Image resolution: <0.23 nm, Electro probe size: <0.3 nm, Magnification: 25–1,030,000 \times , Specimen double tilting: $\pm 40^\circ/\pm 20^\circ$). The catalyst sample was dispersed in ethanol solution and the suspension was carried out using ultrasonic bath for 30 min. The resulting solution was deposited on copper grid coated with a carbon film, and the alcohol was evaporated. Finally, the sample containing the copper grid was used for the TEM and HRTEM/HAADF STEM analysis. CHNS analysis was carried out using a Fissions EA1108 instrument for the determination of the amount of accumulated carbon on the surface of the catalyst after the reaction. The Pt, Sn and K were determined by atomic absorption spectroscopy (AAS) and inductively coupled plasma-atomic emission spectrometer (ICP-AES).

2.3. Activity measurement

The prepared catalysts were first crushed and sieved. The final particle sizes were between 80–140 mesh before the activity test. The n-butane dehydrogenation was carried out at 823 K at atmospheric pressure using 0.1 g of the catalyst after the H₂ reduction. The internal diameter of a fixed bed tubular quartz reactor was 10 mm, and the catalyst bed length between the quartz wool layers in the reactor was approximately 3–4 mm. Before each experiment, the sample was reduced in a pure hydrogen (99.99%) flow (30 mL min⁻¹). The temperature during the reduction was increased slowly from room temperature to 823 K (10 K min⁻¹) and maintained at 823 K for 2 h. After the reduction, H₂:N₂:n-C₄H₁₀ feed gases with a molar ratio of 1.0:1.0:1.0 to were introduced into the catalytic reactor for the reaction, and the total gas flow rate was kept constant at 30 mL min⁻¹ (GHSV: 18,000 mL/g_{cat}/h). The products and reactants were analyzed with an on-line GC (FID detector, Series M 600D, South Korea) equipped with a capillary column (GS-Alumina, Agilent Technologies, USA, i.d.: 0.53 mm, length: 50 m).

3. Results and discussion

3.1. Catalysts characterization

3.1.1. Physical properties of the catalyst

Figs. 1 and 2 show the calcined and reduced XRD patterns of (PtSn)_{1.5} catalyst with different amount of K loadings. No XRD peaks from Pt/PtO or Sn/SnO₂ or K phases were not observed in the calcined catalysts (Fig. 1). Only θ -Al₂O₃ phases appeared at 2 θ -values of 31.05°, 33.05°, 37.15°, 39.52°, 45.10°, 48.00°, 60.20° and 67.58° (ICDD file no.: 47-1771), it is because the metal components were highly dispersed on the support and/or too small to be detected by XRD techniques. The 2 θ values of Pt were at 39.76°, 46.24° and 67.45° (ICDD file no.: 04-0802), and those of Sn were at 15.57°, 16.35°, 22.10°, 27.64° and 28.99° (ICDD file no.: 19-1365). No characteristic peaks of Pt/PtO_x and Sn/SnO_x were observed in the XRD patterns of the reduced potassium doped (PtSn)_{1.5} catalysts, too (Fig. 2). The reduced mono- and bimetallic potassium doped (PtSn)_{1.5} catalysts showed θ -Al₂O₃ (ICDD file no.: 47-1771) and PtSn (ICDD file no.: 25-0614) phases with the 2 θ -values at 25.08°, 30.07° and 41.88° with hexagonal structure, indicating the formation of PtSn alloy during the reduction. Additionally, no diffraction peaks assigned to the crystalline potassium were detected, suggesting that potassium species were highly dispersed on θ -Al₂O₃ support.

Table 1 shows the physical properties such as BET surface area and pore size distribution. The loading amount (Pt, Sn and K) of the prepared catalysts were analyzed using AAS/ICP analysis. The BET surface area, pore volume and average pore diameter of θ -Al₂O₃ were 98 m² g⁻¹, 0.361 cm³ g⁻¹ and 14.6 nm, respectively. The surface areas of the calcined, reduced and used (PtSn)_{1.5} catalyst

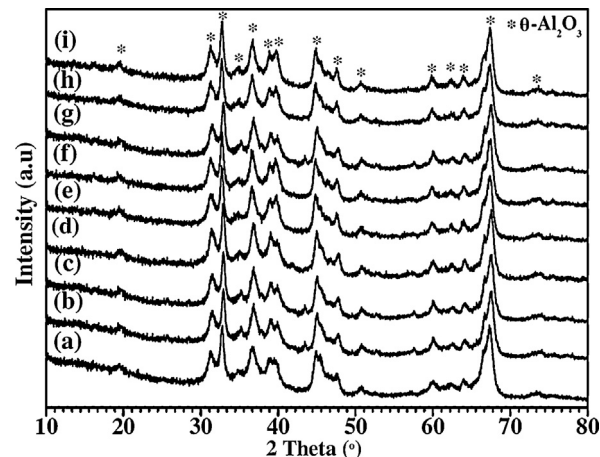


Fig. 1. XRD profiles of the calcined PtSn/ θ -Al₂O₃ (with and without K) catalysts. (a) θ -Al₂O₃, (b) K_{0.95}(Sn)_{1.5}, (c) K_{0.9}(Pt)_{1.5}, (d) (PtSn)_{1.5}, (e) K_{0.4}(PtSn)_{1.5}, (f) K_{0.7}(PtSn)_{1.5}, (g) K_{0.95}(PtSn)_{1.5}, (h) K_{1.2}(PtSn)_{1.5} and (i) K_{1.45}(PtSn)_{1.5}.

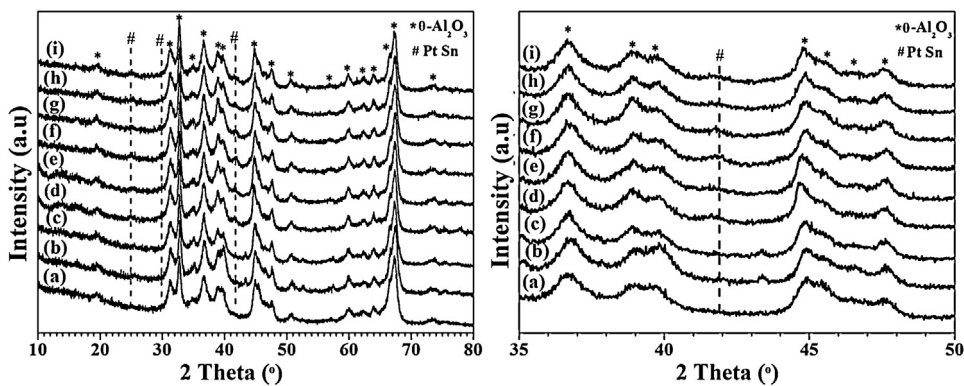


Fig. 2. XRD profiles of the reduced PtSn/θ-Al₂O₃ (with and without K) catalysts; (a) θ-Al₂O₃, (b) K_{0.95}(Sn)_{1.5}, (c) K_{0.9}(Pt)_{1.5}, (d) (PtSn)_{1.5}, (e) K_{0.4}(PtSn)_{1.5}, (f) K_{0.7}(PtSn)_{1.5}, (g) K_{0.95}(PtSn)_{1.5}, (h) K_{1.2}(PtSn)_{1.5} and (i) K_{1.45}(PtSn)_{1.5}.

samples were 86, 82 and 84 m² g⁻¹, respectively. The surface areas of the samples containing potassium were about 79–81 m² g⁻¹. The BET surface area of the (PtSn)_{1.5} catalyst was not so much changed with an increase in potassium content. The pore volume (327 to 297 cm³ g⁻¹) and pore size (15.1 to 14.7 nm) were slightly varied with the increase in potassium content.

3.1.2. NH₃-TPD studies

Fig. 3 shows the NH₃ TPD profiles of θ-Al₂O₃, (PtSn)_{1.5} and 1.0 wt.% of K, Ca, Na and Li supported (PtSn)_{1.5} catalysts. The catalytic activity of *n*-butane dehydrogenation reaction was mainly related to the acidity of the catalysts. All the NH₃ TPD profiles were de-convoluted using Lorentzian–Gaussian functions. Table 2 shows the NH₃ uptakes at different temperatures for the prepared samples. All the samples exhibited three peaks. The peak (I) at 464–480 K is assigned as weak acidic sites, the peak (II) at 504–522 K and 557–587 K can be attributed to medium acidic sites, and the final peak (III) at 613–692 K can be considered as strong acidic sites [5]. The peaks at 760–973 K were assigned as desorption of the strongly adsorbed water or as de-hydroxylation (Fig. 3). For the confirmation of the peaks at 760–973 K, temperature programmed desorption with θ-Al₂O₃ was performed without NH₃ adsorption. The helium gas was introduced into the reactor with the alumina support at 373 K for 1 h. Then, the temperature was ramped from 323 to 1073 K with a heating rate of 10 K min⁻¹ under the flow of helium (30 mL min⁻¹). The water peak was clearly observed at 760–973 K and the peak profile was shown in Fig. 3(a1). The (PtSn)_{1.5} catalysts showed the total NH₃ uptake of 0.526 mmol (g cat)⁻¹, which is low as compared with the support θ-Al₂O₃ (0.664 mmol (g cat)⁻¹). The result indicates that the addition of Pt and Sn on θ-Al₂O₃ decreased the acidic sites of the support [18]. The NH₃ TPD results of alkali metals such as K, Ca, Na and Li doped (PtSn)_{1.5} were also studied, and the results were also shown in Table 2. The addition of K to (PtSn)_{1.5} decreased the total NH₃ uptake (0.315 mmol (g cat)⁻¹). The order of the total NH₃ uptakes were as follows: θ-Al₂O₃ > (PtSn)_{1.5} > Li_{0.95}(PtSn)_{1.5} > Na_{0.95}(PtSn)_{1.5} > Ca_{0.95}(PtSn)_{1.5} > K_{0.95}(PtSn)_{1.5}. Zhang et al. and Bariås et al. reported that the addition of K or Sn reduced the acidic sites of the support due to its basic character [27,28]. The experimental results clearly showed that the addition of K to (PtSn)_{1.5} suppressed the acidity, minimizing isomerization products in *n*-butane dehydrogenation reaction as shown in Table 7.

3.1.3. Temperature programmed reduction studies

Fig. 4 shows the TPR profiles of the K_{0.9}(Pt)_{1.5}, K_{0.95}(Sn)_{1.5}, (PtSn)_{1.5} (without K) and different wt.% of potassium doped bimetallic (PtSn)_{1.5} catalysts and Table 3 shows the reduction

temperature, hydrogen consumption and percentage of the reduction of potassium doped mono- and bimetallic catalysts. All the TPR profiles were de-convoluted using Lorentzian–Gaussian functions. The mono metallic K_{0.9}(Pt)_{1.5} (Fig. 4a) catalyst showed the low temperature reduction peak at 478 K with a small shoulder at 400 K, which was assigned as the reduction of the Pt species in the weak interaction with the support. The other peak at 521 and 633 K was assigned to the reduction of the Pt species in the strong interaction with the support [23]. The reduction peaks at 714 and 823 K can be attributed to oxychlorinated Pt species. [24,29,30]. A small reduction peak for a finely dispersed Sn species at 530 K appeared with K_{0.95}(Sn)_{1.5} catalyst (Fig. 4b). The broad reduction peak at 712 and 752 K could be due to the reduction of Sn⁴⁺/Sn²⁺ and/or Sn²⁺/Sn⁰ species, respectively [17,31]. The broad peak at 886 K can be assigned to the reduction of Sn²⁺ to Sn⁰ in a high interaction with the support [5,32].

It is observed that the (PtSn)_{1.5} without K (Fig. 4c) showed the reduction peaks at 476, 548, 677, and 946 K. The new reduction peak at 476 K (α) can be assigned to the co-reduction of the Pt species with Sn species, which is mainly related to the Pt species in the weak interaction with the support. The peak at 548 (β) can be assigned to the co-reduction of the Pt species with Sn species, which is related mainly to the Pt species in the strong interaction with the support. The reduction peak at 677 (γ) can be assigned mainly to the reduction of isolated Sn⁴⁺/Sn²⁺ and/or Sn²⁺/Sn⁰ species. The reduction peak at 946 K (δ) can be assigned mainly to the reduction of Sn²⁺/Sn⁰ species with the strong interaction with the support, respectively. The K_{0.4}(PtSn)_{1.5} catalyst (Fig. 4d) showed the reduction peaks at 520, 579, 753 and 787 K. The reduction peaks at 520 K (α) and 579 K (β) can be assigned to the reduction of the Pt with Sn and K species [27]. The reduction peaks at 753 and 787 K (γ) can be assigned mainly to the reduction of Sn⁴⁺/Sn²⁺ and/or Sn²⁺/Sn⁰ species, respectively. The K_{0.7}(PtSn)_{1.5} (Fig. 4e) catalyst showed α , β , γ , and δ peak at 515, 611, 786 and 809 K. The K_{0.95}(PtSn)_{1.5} (Fig. 4f) catalyst also showed α , β , γ , and δ peak at 503, 688 and 830 K. The similar trend was observed in K_{1.2}(PtSn)_{1.5} and K_{1.45}(PtSn)_{1.5} (Fig. 4g and h) catalyst. The reduction peak at low temperature (α and β) shifted towards higher temperature with the addition K. The reduction peak area of Sn species at δ increased and the reduction temperature decreased with the addition of K, indicating that the addition of potassium promoted the reduction of Sn species [14]. The hydrogen consumption increased with the increase of potassium content because the reduction amount of Sn species increased with the addition of potassium (Table 3). The experimental result indicates that the excess addition of K weakened the interaction between Sn and the support, which caused low catalytic activity and stability. The addition of K could also give an effect on the interaction between Pt and Sn as Perak et al. [33]

Fig. 3. NH₃-TPD profiles of the calcined PtSn/θ-Al₂O₃ ((PtSn)_{1.5} and K, Ca, Na and Li doped (PtSn)_{1.5}) catalysts. (a) θ-Al₂O₃ (without NH₃), (a) θ-Al₂O₃, (b) (PtSn)_{1.5}, (c) K_{0.95}(PtSn)_{1.5}, (d) Ca_{0.95}(PtSn)_{1.5}, (e) Na_{0.95}(PtSn)_{1.5} and (f) Li_{0.95}(PtSn)_{1.5}.

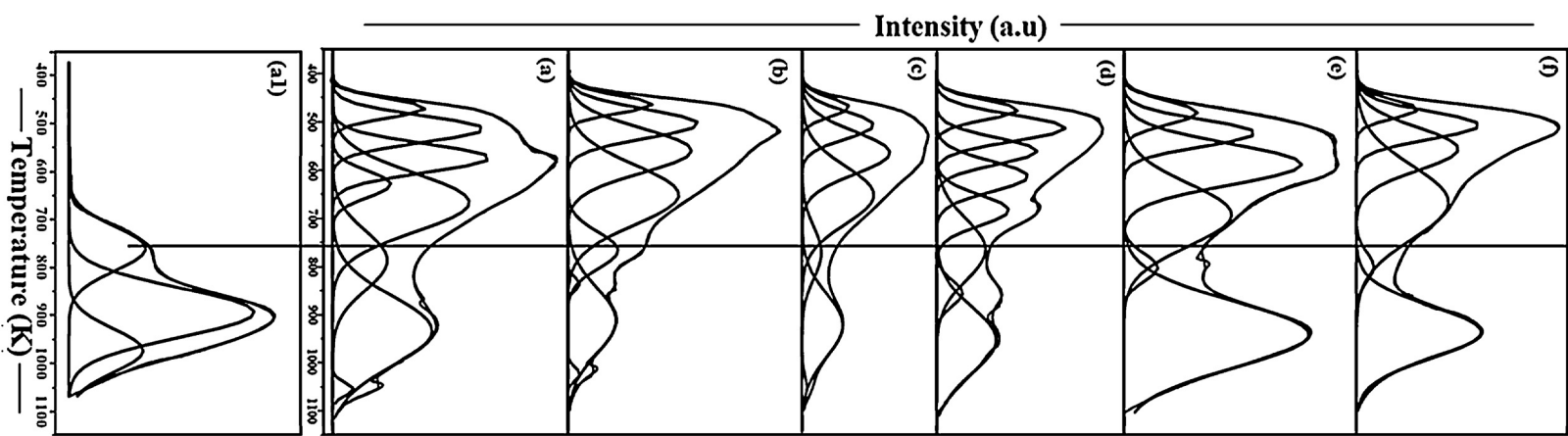


Table 2
NH₃-TPD results of θ-Al₂O₃, (PtSn)_{1.5} and different alkali metals supported on (PtSn)_{1.5}/θ-Al₂O₃ catalysts.

Catalysts	Weak acidic sites (I)		Medium acidic sites (II)		Strong acidic sites (III)		Total NH ₃ uptake/mmol (g cat) ⁻¹
	Temperature (K); Percentage (%)	NH ₃ uptake/mmol (g cat) ⁻¹	Temperature (K); Percentage (%)	NH ₃ uptake/mmol (g cat) ⁻¹	Temperature (K); Percentage (%)	NH ₃ uptake/mmol (g cat) ⁻¹	
θ-Al ₂ O ₃	472; (9)	0.060	512; (20), 575; (22)	0.133, 0.146	629; (8), 667; (41)	0.053, 0.272	0.664
(PtSn) _{1.5}	464; (9)	0.047	504; (22), 560; (31)	0.116, 0.163	652; (38)	0.200	0.526
K _{0.95} (PtSn) _{1.5}	470; (8)	0.025	507; (18), 564; (35)	0.057, 0.110	652; (39)	0.123	0.315
Ca _{0.95} (PtSn) _{1.5}	475; (13)	0.058	513; (26), 561; (21)	0.116, 0.093	613; (22), 683; (18)	0.098, 0.080	0.445
Na _{0.95} (PtSn) _{1.5}	480; (9)	0.042	522; (18), 587; (38)	0.085, 0.179	692; (35)	0.165	0.471
Li _{0.95} (PtSn) _{1.5}	474; (7)	0.034	508; (21), 557; (28)	0.102, 0.135	667; (44)	0.213	0.484

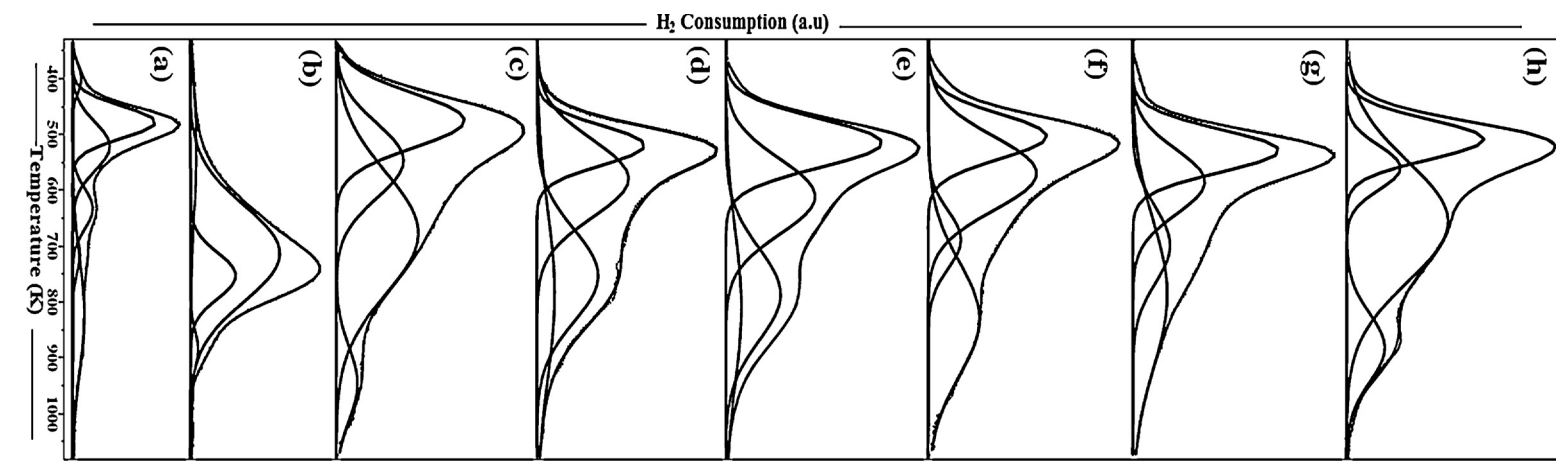


Fig. 4. TPR profiles of the calcined PtSn/θ-Al₂O₃(with and without K) catalysts. (a) K_{0.9}(Pt)_{1.5}, (b) K_{0.95}(Sn)_{1.5}, (c) (PtSn)_{1.5}, (d) K_{0.4}(PtSn)_{1.5}, (e) K_{0.7}(PtSn)_{1.5}, (f) K_{1.2}(PtSn)_{1.5} and (h) K_{1.45}(PtSn)_{1.5}.

Table 3

H₂-TPR profiles of mono and bimetallic 1.5 wt.% (PtSn)/θ-Al₂O₃ with different potassium loadings.

Catalysts	α Peak		β Peak		γ Peak		δ Peak	
	Temperature (K); Percentage (%)	H ₂ consumption/mmol H ₂ (g cat) ⁻¹	Temperature (K); Percentage (%)	H ₂ consumption/mmol H ₂ (g cat) ⁻¹	Temperature (K); Percentage (%)	H ₂ consumption/mmol H ₂ (g cat) ⁻¹	Temperature (K); Percentage (%)	H ₂ consumption/mmol H ₂ (g cat) ⁻¹
(PtSn) _{1.5}	476; (29)	0.050	548; (22)	0.040	677; (43)	0.080	946; (6)	0.010
K _{0.4} (PtSn) _{1.5}	520; (21)	0.044	579; (36)	0.075	753; (28), 787; (15)	0.059, 0.031	–	–
K _{0.7} (PtSn) _{1.5}	515; (35)	0.079	611; (31)	0.070	786; (23)	0.052	809; (11)	0.025
K _{0.95} (PtSn) _{1.5}	503; (26)	0.062	569; (38)	0.091	688; (9)	0.022	830; (27)	0.065
K _{1.2} (PtSn) _{1.5}	529; (35)	0.089	584; (25)	0.064	698; (15), 787; (25)	0.038, 0.064	–	–
K _{1.45} (PtSn) _{1.5}	508; (24)	0.065	559; (10)	0.027	655; (54)	0.146	882; (12)	0.032
K _{0.9} (Pt) _{1.5}	400; (4), 478; (37)	0.0038, 0.035	521; (25), 633; (11)	0.023, 0.010	714; (4)	0.0038	823; (19)	0.018
K _{0.95} (Sn) _{1.5}	530; (6)	0.008	–	–	712; (73), 752; (18)	0.103, 0.025	886; (3)	0.004

Table 4

CO chemisorptions and amount of coke deposited on the catalyst after *n*-butane dehydrogenation reaction at 823 K for 5 h.

Catalysts/wt.%	Amount of CO adsorbed in/cm ³ STP (g cat) ⁻¹	Pt dispersion/%	Pt surface area/m ² (g cat) ⁻¹	Average particle size (nm)		Coke amount (wt.%) ^c
				CO ^a	TEM ^b	
(PtSn) _{1.5}	0.112	7.5	0.241	15.1	7.1	0.8
K _{0.4} (PtSn) _{1.5}	0.100	6.7	0.216	16.8	8.6	0.5
K _{0.7} (PtSn) _{1.5}	0.096	6.4	0.206	17.6	9.8	0.4
K _{0.95} (PtSn) _{1.5}	0.090	6.1	0.194	18.7	10.5	0.3
K _{1.2} (PtSn) _{1.5}	0.051	3.4	0.110	33.0	16.4	1.2
K _{1.45} (PtSn) _{1.5}	0.033	2.2	0.072	50.3	23.5	1.8
K _{0.9} (Pt) _{1.5}	0.082	5.3	0.176	21.4	15.4	2.9

^a Calculated from CO chemisorptions.

^b Mean particle size of the metal catalyst from TEM images using at least 30 visible particles.

^c From elemental analysis.

suggested that the addition of Sn and K to Pt could lead to a direct interaction between Pt with Sn and K. To investigate the K effect on active Pt metal, CO chemisorption study was performed.

3.1.4. CO chemisorption study

Table 4 shows the Pt surface areas (MSA), Pt dispersions (D) and particle sizes (PS) of the (PtSn)_{1.5} and potassium doped (PtSn)_{1.5} catalysts by CO chemisorption. The mono metallic K_{0.9}(Pt)_{1.5} catalyst exhibited a low Pt dispersion. The bimetallic (PtSn)_{1.5} catalyst showed the highest Pt dispersion and Pt surface area. The Pt dispersion of (PtSn)_{1.5} catalyst slightly decreased with an increase in amount of potassium. However, the Pt metal dispersion abruptly decreased when potassium was added to the (PtSn)_{1.5} catalyst more than 1.2 wt.%. The potassium addition below 1.0 wt.% rarely covered the exposed Pt surface, indicating the presence of the chemical interaction with Pt, while that above 1.0 wt.% significantly covered the Pt surface resulting in low Pt dispersion. As previously discussed, the high Pt dispersion of the (PtSn)_{1.5} can be ascribed due to the prevention of Pt migration by the PtSn alloy formation at low reduction temperature [26].

3.1.5. HAADF STEM and corresponding EDX mapping

The XRD pattern did not show any metal or metal oxides (Pt/PtO_x or Sn/SnO_x) or potassium peaks in the calcined catalysts, and only peaks of θ -Al₂O₃ phase were observed. To identify the structures of the Pt, Sn, K and PtSn particles on θ -Al₂O₃, the K_{0.95}(PtSn)_{1.5} sample was characterized using a FEI microscopy in STEM mode. Fig. 5(a) and (b) show typical high-angle annular dark-field scanning TEM (HAADF STEM) images and the corresponding EDS maps of the calcined and reduced K_{0.95}(PtSn)_{1.5} catalysts, respectively. Fig. 5(a) shows the HAADF STEM-EDS compositional maps of the calcined K_{0.95}(PtSn)_{1.5} catalyst. The distribution of the Pt, Sn and K particles was clearly visible. The Pt particles were scattered on the support, while the Sn and K particles were uniformly well distributed as shown in the EDS mapping. Fig. 5(b) also shows the HAADF STEM-EDS compositional maps of the reduced K_{0.95}(PtSn)_{1.5} catalyst. The distributions of Pt, Sn and K particles were also visible. The Pt, Sn and K particles on the reduced K_{0.95}(PtSn)_{1.5} catalyst were observed at the same position. The number of Pt particles of the calcined K_{0.95}(PtSn)_{1.5} sample decreased after the reduction, indicating the Pt particles were sintered. However, the highly dispersed Sn and K particles on the calcined K_{0.95}(PtSn)_{1.5} sample were migrated to the Pt particles during the reduction. From HAADF STEM and corresponding EDX mapping, it is clear that Pt, Sn and K are on the same position after the reduction. The experimental results suggest the PtSn alloy can form during the reduction step and the major of potassium are not on the support, but on the PtSn particles. Therefore, it is concluded that the main potassium effect on the PtSn catalysts are closely related to the interaction with Pt. The

acidic sites of Pt particles can be inhibited by the interaction with potassium.

3.1.6. Transmission electron microscopy (TEM) studies

The Fig. 6 shows TEM images and particle size distribution of the reduced K_{x,x}/(PtSn)_{1.5} catalysts. The TEM images exhibited that the Pt particle sizes of the reduced K_{0.9}(Pt)_{1.5}, K_{0.4}(PtSn)_{1.5}, K_{0.7}(PtSn)_{1.5}, K_{0.95}(PtSn)_{1.5}, K_{1.2}(PtSn)_{1.5} and K_{1.45}(PtSn)_{1.5} catalysts were about 15.4, 8.6, 9.8, 10.5, 16.4 and 23.5 nm, respectively. The Pt particles size of the (PtSn)_{1.5} catalyst without potassium was the smallest among the prepared catalysts, which is corresponded with the CO chemisorption results. The Pt particle size increased and the Pt metal dispersion decreased with an increase in potassium content on the (PtSn)_{1.5} catalyst (Table 4). The average Pt particle sizes by TEM analysis were approximately half of those from the chemisorption data (Table 4). A conventional CO/Pt_{atm} of 1.0 was used for the Pt particle size calculation. In the supported Pt/Al₂O₃ catalysts, the CO/H ratio for a Pt atom was estimated as 0.83–0.96 [34]. In the well-dispersed catalysts, a CO/H ratio of 0.7 was reported for an H/Pt ratio of 1.0, which was due to the CO bridged bonding of 50% on Pt [35]. Here, the Pt metal particle size on the bimetallic catalysts by TEM analysis will be equivalent to that by CO chemisorption, if the CO/Pt ratio is 0.5.

Fig. 7 shows the HRTEM micrograph of the calcined and reduced K_{0.95}(PtSn)_{1.5} catalyst, indicating the presence of individual particles with clear lattice fringes. The fast Fourier transform (FFT) was applied to calculate the lattice spacing of the crystallite. The FFT image (Fig. 7(a)) of the calcined K_{0.95}(PtSn)_{1.5} catalyst exhibited the lattice spacing of 0.236 nm corresponding to the (1 1 1) reflection planes of the Pt, respectively. The FFT images of the reduced K_{0.95}(PtSn)_{1.5} catalyst (Fig. 7(b)) showed a spacing of 0.218 nm, corresponding to the (1 0 2) planes of the PtSn alloy.

3.2. Catalytic activity

3.2.1. Effect of potassium on 1.5 wt.% PtSn supported θ -Al₂O₃ catalysts

Fig. 8 shows the conversion of *n*-butane with respect to the reaction time on the (PtSn)_{1.5} catalyst, the potassium doped (Pt)_{1.5}, (Sn)_{1.5}, and the potassium doped (PtSn)_{1.5} catalysts. Table 5 shows the initial and final (X_i and X_f , measured at 30 to 300 min. of the reaction time) conversion, *n*-C₄⁺ selectivity and *n*-C₄⁺ yields of the tested catalysts. The reaction was carried out at 823 K for 5 h in *n*-butane dehydrogenation. In the product distribution, 1,3-butadiene was produced by the dehydrogenation of *n*-butenes during *n*-butane dehydrogenation. The selectivity to 1,3-butadiene was limited by the thermodynamic equilibrium in the reaction condition. The products of C₁–C₃ included methane, ethane, propane and propylene, which could be produced on the hydrocracking sites on the Pt metal species. The cracking products were the highest on

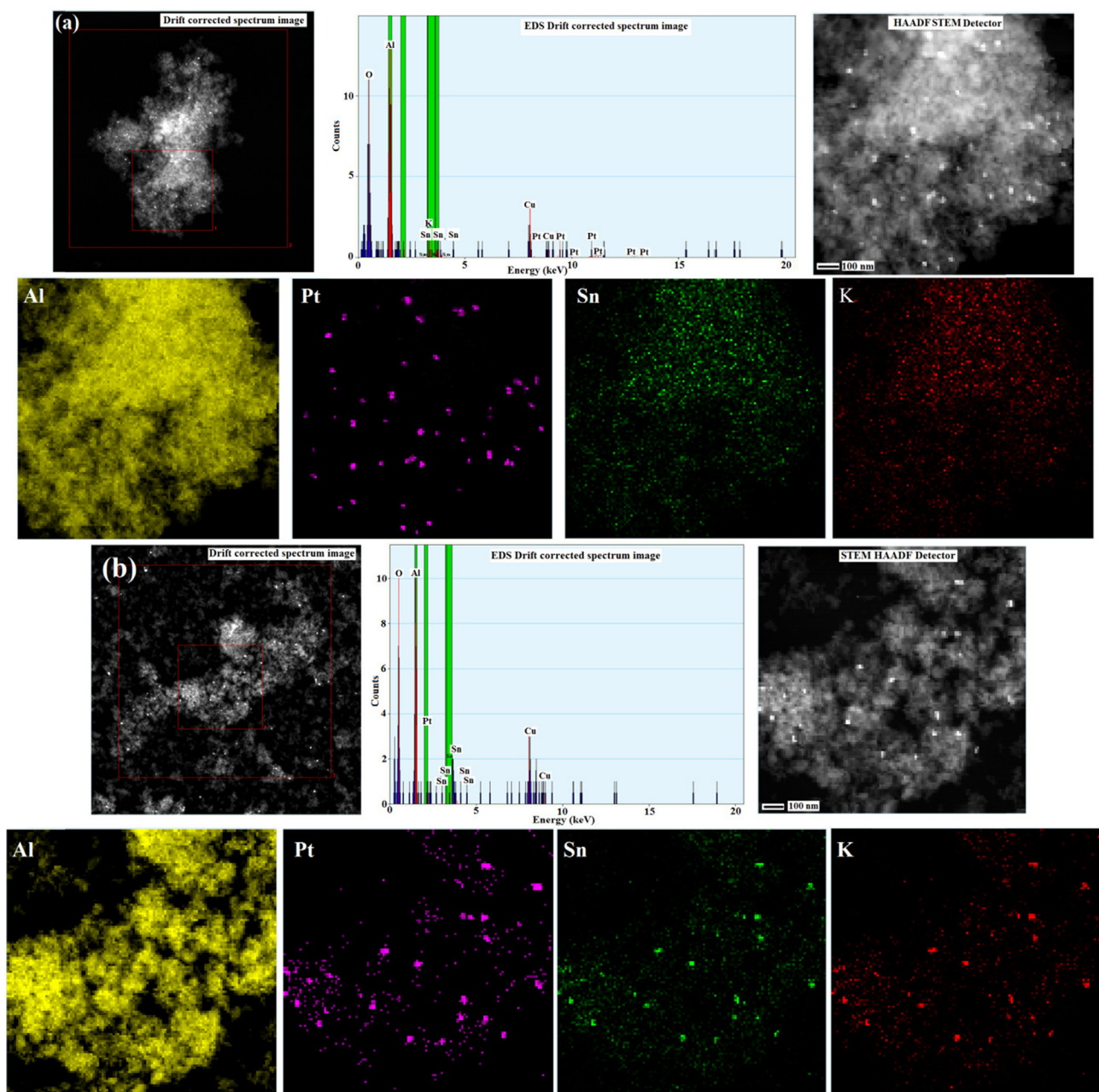


Fig. 5. The high angle annular dark-field scanning TEM (HAADF STEM) images and the corresponding EDS maps of the (a) calcined and (b) reduced 0.95 wt.% potassium doped $(\text{PtSn})_{1.5}$ catalyst.

Table 5

Activity and deactivation parameter of 1.5 wt.% $(\text{PtSn})/\theta\text{-Al}_2\text{O}_3$ catalysts (with and without K) for *n*-butane dehydrogenation reaction at 823 K and a GHSV of 18,000 mL/g_{cat}/h.

Catalysts (wt.%)	Conversion (%)		Deactivation parameter* (ΔX)	Selectivity (S_i/S_f) (%)				Yield of <i>n</i> -C ₄ " (Y_f) (%)		
	Initial (X_i)	Final (X_f)		$C_1\text{-}C_3$		$n\text{-C}_4"$				
				1-Butene	2-Butene	1-Butene	2-Butene			
$(\text{PtSn})_{1.5}$	46.7	43.6	6.63	1.7/1.7	30.9/34.5	45.8/51.9	18.3/8.0	3.3/3.9		
$K_{0.4}(\text{PtSn})_{1.5}$	41.9	39.5	5.72	1.1/1.2	37.5/37.2	55.8/56.0	1.8/1.6	3.8/4.0		
$K_{0.7}(\text{PtSn})_{1.5}$	40.4	38.4	4.95	1.5/1.5	37.6/37.2	55.1/55.7	1.8/1.6	4.0/4.0		
$K_{0.95}(\text{PtSn})_{1.5}$	44.1	42.8	2.95	1.6/1.5	36.1/37.1	56.4/55.8	1.6/1.3	4.3/4.3		
$K_{1.2}(\text{PtSn})_{1.5}$	33.5	27.3	18.51	1.4/3.1	37.0/33.1	55.3/55.7	1.5/3.0	4.8/5.1		
$K_{1.45}(\text{PtSn})_{1.5}$	13.2	9.5	28.03	3.8/5.4	31.0/28.0	56.2/56.0	4.4/5.9	4.6/4.7		
$K_{0.9}(\text{Pt})_{1.5}$	24.1	16.6	31.12	6.5/7.5	33.7/32.1	51.3/52.0	5.4/5.0	3.0/3.4		
$K_{0.95}(\text{Sn})_{1.5}$	0.95	0.95	—	55.4/56.9	2.8/2.6	5.9/5.3	35.9/35.2	0.0/0.0		

*: $\Delta X = (X_i - X_f)/X_i \times 100$.

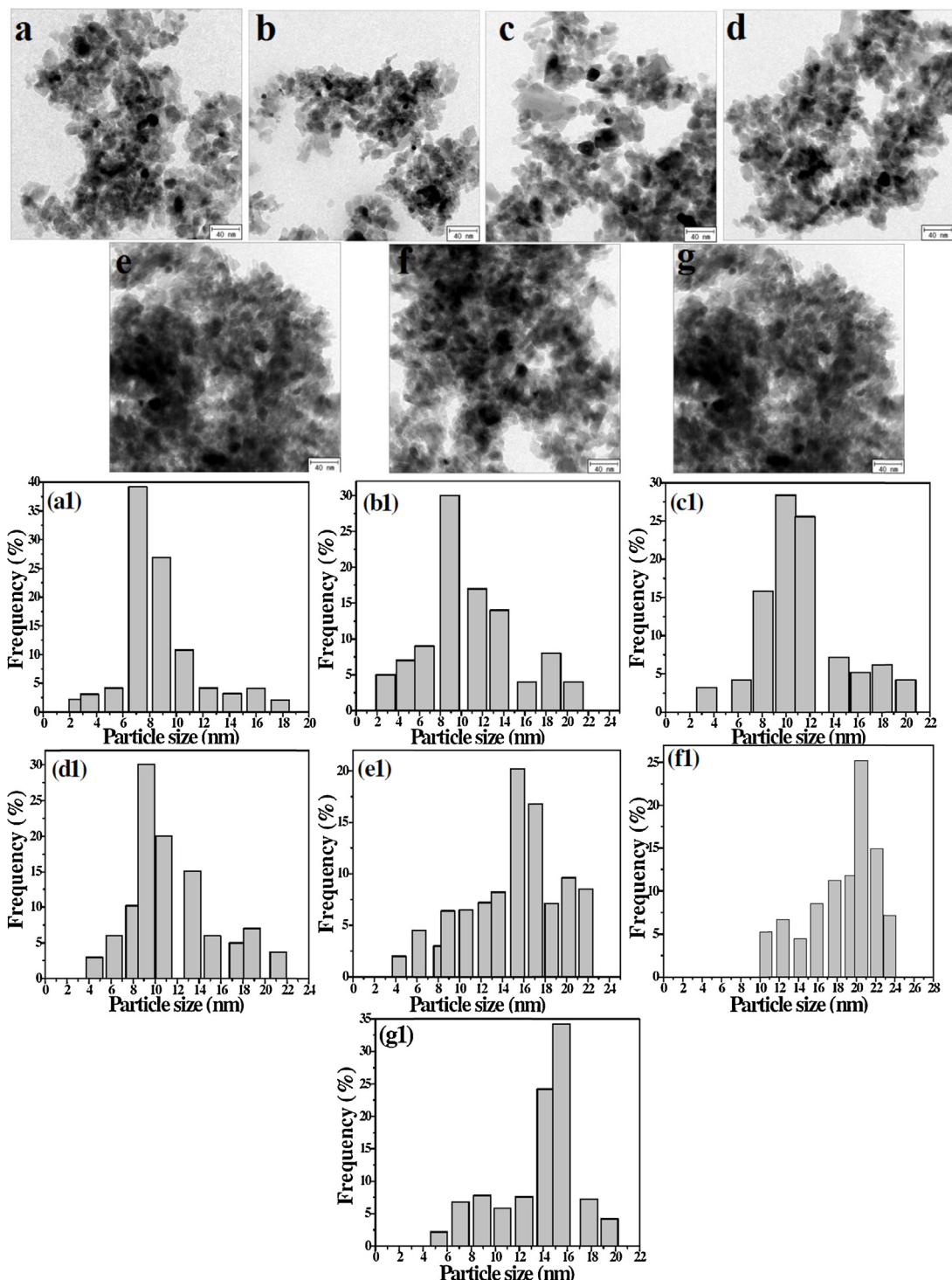


Fig. 6. TEM images of the reduced PtSn/θ-Al₂O₃(with and without) catalysts. (a,a1) (PtSn)_{1.5}, (b,b1) K_{0.4}(PtSn)_{1.5}, (c,c1) K_{0.7}(PtSn)_{1.5}, (d,d1) K_{0.95}(PtSn)_{1.5}, (e,e1) K_{1.2}(PtSn)_{1.5}, (f,f1) K_{1.45}(PtSn)_{1.5} and (g,g1) K_{0.9}(Pt)_{1.5}.

the K_{0.9}(Pt)_{1.5} catalyst. The cracking sites on the Pt catalyst was little influenced by the potassium addition, but was blocked by the Sn addition as shown in Table 5. The selectivity to C₁–C₃ of (PtSn)_{1.5} catalyst was not so much changed with the addition of potassium, but rather increased with the potassium addition more than 1.5 wt%.

Isobutane was a main isomerization product in *n*-butane dehydrogenation. The isomerization is due to the acid sites of the catalysts. The acid sites can be present on both Pt sites and support.

It is clear that the potassium addition suppressed the isomerization sites of the (PtSn)_{1.5} catalyst as shown in Table 5. The selectivity to the isobutane decreased with a potassium addition up to 1 wt%, but rather increased with the further potassium addition. If the potassium suppressed the acid sites on the support, the selectivity to isobutene should have maintained at low level even at the potassium addition more than 1.5 wt%. As shown in Fig. 4, most of potassium particles are not on the support, but on Pt particles, indicating that the potassium suppressed the acidic sites on the

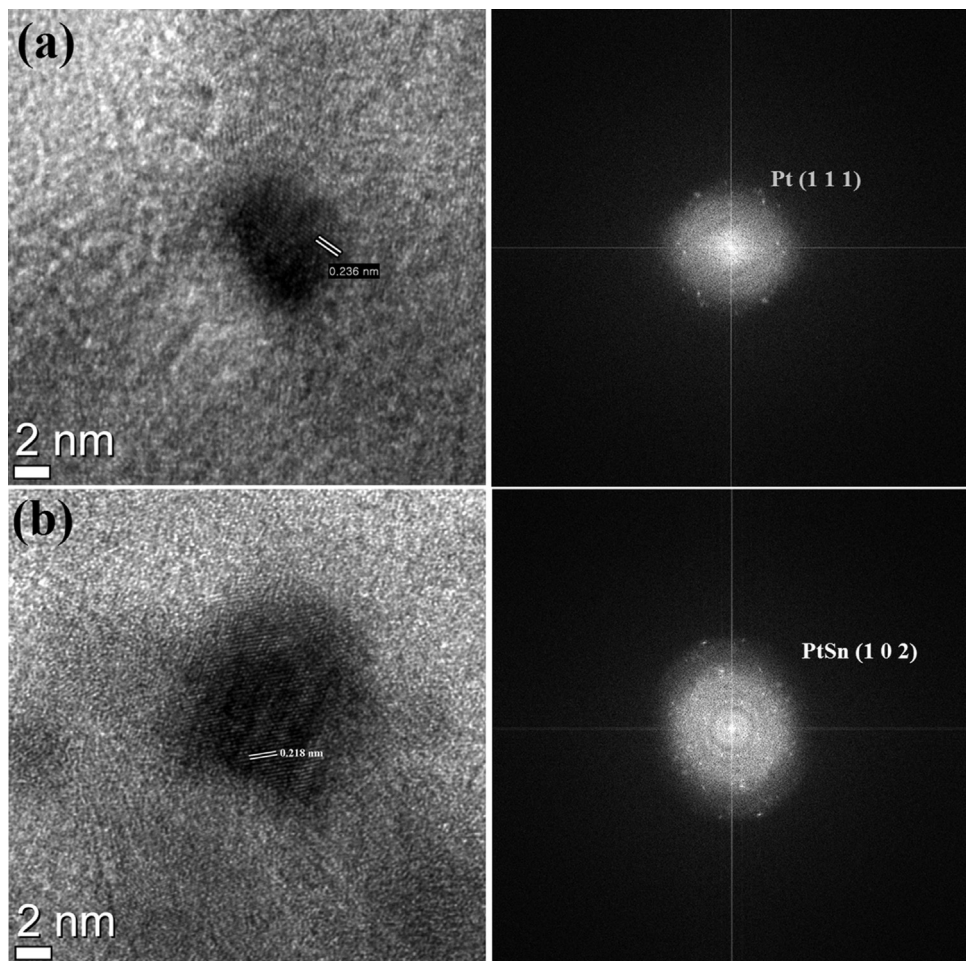


Fig. 7. HRTEM micrographs and corresponding FFTs of the (a) $K_{0.95}(PtSn)_{1.5}$ -calcined and (b) $K_{0.95}(PtSn)_{1.5}$ -reduced 0.95 wt.% potassium doped $PtSn/\theta\text{-Al}_2\text{O}_3$ catalysts.

Pt particles. It has been known that the acid sites for isomerization were related with chlorine presence on the Pt/alumina catalyst [36–38]. In our reaction temperature, oxychlorinated platinum was reduced during the reduction as shown in Fig. 4. It was shown that the hydro-dechlorination can induce the strong acid sites on the catalysts [37] which were titrated with potassium, resulting in low isobutene yield.

The initial conversions of $(PtSn)_{1.5}$, $K_{0.4}(PtSn)_{1.5}$, $K_{0.7}(PtSn)_{1.5}$, $K_{0.95}(PtSn)_{1.5}$, $K_{1.2}(PtSn)_{1.5}$, $K_{1.45}(PtSn)_{1.5}$, $K_{0.9}(Pt)_{1.5}$ and $K_{0.95}(Sn)_{1.5}$ catalysts were 46.7, 41.9, 40.4, 44.1, 33.5, 13.2, 24.1 and 0.95%, respectively. The conversion of each catalyst after 5 h decreased to 43.6, 39.5, 38.4, 42.8, 27.3, 9.5, 16.6 and 0.95%, respectively. The catalysts listed in order of the $n\text{-C}_4$ conversion for 5 h reaction at 823 K were as follows:

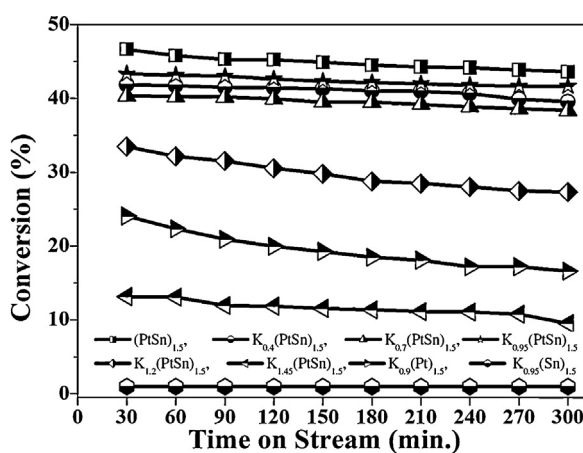


Fig. 8. Conversion vs time on stream on $(PtSn)_{1.5}$ catalyst (with and without K) with different amount of potassium for n -butane dehydrogenation reaction at 823 K and a GHSV of 18,000 $\text{mL/g}_{\text{cat}}/\text{h}$.

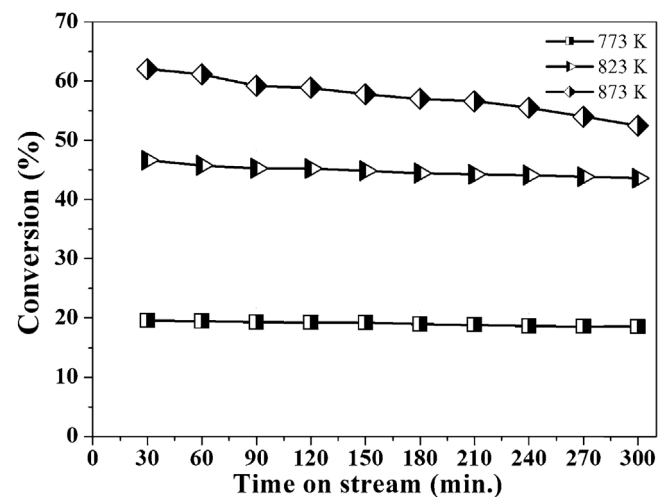


Fig. 9. Stability test on $(PtSn)_{1.5}$ and $K_{0.95}(PtSn)_{1.5}$ catalyst at 823 K for 15 h for the n -butane dehydrogenation reaction at 823 K and a GHSV of 18,000 $\text{mL/g}_{\text{cat}}/\text{h}$.

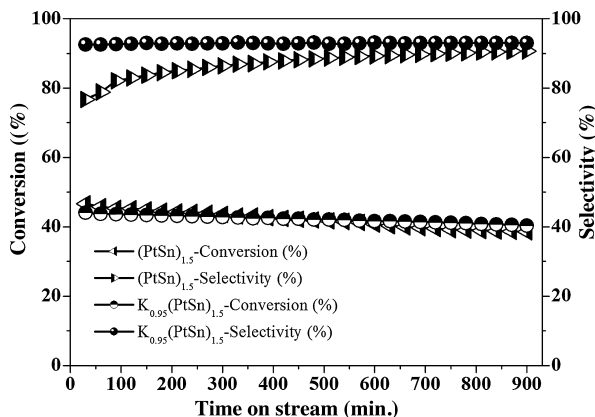


Fig. 10. Conversion vs time on stream on K_{0.95}(PtSn)_{1.5} catalyst with different temperatures for the n-butane dehydrogenation reaction at 823 K and a GHSV of 18,000 mL/g_{cat}/h.

(PtSn)_{1.5} > K_{0.95}(PtSn)_{1.5} > K_{0.4}(PtSn)_{1.5} > K_{0.7}(PtSn)_{1.5} > K_{1.2}(PtSn)_{1.5} > K_{0.9}(Pt)_{1.5} > K_{1.45}(PtSn)_{1.5}. The conversion is closely related to the Pt dispersion except K_{0.95}(PtSn)_{1.5}. The K_{0.95}(PtSn)_{1.5} showed the optimized composition for the potassium addition on the (PtSn)_{1.5} catalyst. Veldurthi et al. reports that the improvement of catalytic activity was mainly related to the Pt dispersion, Pt surface area and particle size of the catalysts [39]. However, the catalysts listed in the order of the stability from the deactivation parameters were as follows: K_{0.95}(PtSn)_{1.5} > K_{0.7}(PtSn)_{1.5} > K_{0.4}(PtSn)_{1.5} > (PtSn)_{1.5} > K_{1.2}(PtSn)_{1.5} > K_{1.45}(PtSn)_{1.5} > K_{0.9}(Pt)_{1.5} > K_{0.95}(Sn)_{1.5}. The deactivation parameters of the prepared catalysts are shown in Table 5 ($\Delta X = 100 \times (X_i - X_f)/X_i$, where X_i is the initial and X_f is the final conversion, respectively). The monometallic K_{0.9}(Pt)_{1.5} showed very high deactivation parameter and the catalyst was strongly deactivated with time on steam was expected. K_{0.9}(Pt)_{1.5} catalyst showed very low Pt dispersion (5.3%) and Pt surface area (0.176 m² (g cat)⁻¹), and a large Pt particles size (>15.4 nm). The coke formation after the reaction was 2.9 wt.%, which was the highest among the prepared catalysts. The deactivation parameters are closely related to the coke amount after 5 h reaction. The coke formation on the catalyst involves several processes such as dehydrogenation condensation, polymerization, and cyclization of hydrocarbon species on the catalyst surface. It was known that the olefinic precursors on the metal active sites migrated to the support, which were converted to polyolefinic or polyaromatic types of coke through condensation and polymerization reaction [2,3,15,17,40]. The relationship between the particle size of the active metal and the amount of carbon deposited on the surface of the support was reported [13,41,42].

The coke deposition on the (PtSn)_{1.5} catalyst was lower than K_{0.9}(Pt)_{1.5}, while that on the (PtSn)_{1.5} catalyst decreased with an increase in the potassium amount up to 1 wt.%. The coke can form on the cracking and isomerization sites on the Pt particles. The coke deposition on Pt catalyst occurred mainly on the cracking sites on the Pt particles and the cracking sites were inhibited by the Sn addition. The potassium could inhibit the acid sites for isomerization on the Pt particles, resulting in decreasing the carbon amount on the (PtSn)_{1.5} catalyst further as shown in Table 4. The stability of (PtSn)_{1.5} catalyst also increased with an increase in the potassium amount up to 1.0 wt.%. The high stability of (PtSn)_{1.5} catalyst with low potassium content is ascribed due to the suppression of the acid sites on the (PtSn)_{1.5} catalyst, while the low stability of (PtSn)_{1.5} catalyst with high potassium content can be due to large Pt particle sizes as shown in Table 4. Additionally, the high selectivity to C₁–C₃ of K_{1.45}(PtSn)_{1.5} indicates that PtSn interaction was weakened by the potassium addition of high content.

The n-C₄⁼ selectivity of the (PtSn)_{1.5} catalyst was 76.7/86.4% for S_i/S_f, while that of the K_{0.95}(PtSn)_{1.5} catalyst was 92.5/92.9%. The high n-C₄⁼ selectivity of the potassium doped (PtSn)_{1.5} catalysts resulted from inhibiting the isomerization sites on the (PtSn)_{1.5} catalyst as discussed previously, because the selectivity to C₁–C₃ was not so much changed with the potassium addition. The potassium contained PtSn alloy particles restrict the sites for cracking, hydrogenolysis, and isomerization, resulting in high n-C₄⁼ selectivity and resistance to the coke formation. Finally, the catalysts listed in the order of the n-C₄⁼ yield were as follows: K_{0.95}(PtSn)_{1.5} > (PtSn)_{1.5} > K_{0.7}(PtSn)_{1.5} > K_{0.4}(PtSn)_{1.5} > K_{1.2}(PtSn)_{1.5} > K_{0.9}(Pt)_{1.5} > K_{1.45}(PtSn)_{1.5}.

3.2.2. Effect of reaction temperature and stability test on K_{0.95}(PtSn)_{1.5} catalyst

The K_{0.95}(PtSn)_{1.5} catalyst showed the highest n-C₄⁼ yield among the prepared catalysts. Fig. 9 shows the butane conversion of K_{0.95}(PtSn)_{1.5} catalyst with respect to the time on stream in the range of 773–873 K, and Table 6 shows the deactivation parameter, butane conversion, n-C₄⁼ selectivity, and n-C₄⁼ yield. The deactivation parameter increased with an increase in the reaction temperature. The n-butane conversion rapidly deactivated at 873 K. The cracking products of C₁–C₃ also increased with an increase in the reaction temperature, resulting in the low n-C₄⁼ selectivity. The higher the reaction temperature, the higher the 1,3-butadiene yield in the thermodynamic point. The reaction at 873 K showed the highest n-C₄⁼ yield after 5 h reaction, but the catalyst was strongly deactivated as compared with other temperatures for n-butane dehydrogenation reaction.

Fig. 10 shows the catalytic activity of the (PtSn)_{1.5} and K_{0.95}(PtSn)_{1.5} catalyst at 823 K for 15 h. The (PtSn)_{1.5} catalyst was deactivated with time on stream more rapidly than the K_{0.95}(PtSn)_{1.5} catalyst. After 15 h, the conversion of n-butane on K_{0.95}(PtSn)_{1.5} catalyst was higher than that on (PtSn)_{1.5}. The initial n-C₄⁼ selectivity of the (PtSn)_{1.5} catalyst were 77%, which steadily increased up to 90% after 15 h. The amount of coke was measured to be about 3.3 wt.% after 15 h. The acid sites of the (PtSn)_{1.5} catalyst were blocked by the coke formation during the reaction, which resulted in the increase of n-C₄⁼ selectivity. On the other hand, the n-C₄⁼ selectivity of the K_{0.95}(PtSn)_{1.5} catalyst (ca. 93%) was not so much changed during the reaction for 15 h, because the potassium blocked the acid sites in advance. The amount of coke on the K_{0.95}(PtSn)_{1.5} catalyst was 0.6 wt.% after 15 h reaction.

3.2.3. Effect of alkali (K, Ca, Na and Li) doped 1.5 wt.% (PtSn) supported θ -Al₂O₃ catalysts

Fig. 11 shows the conversion of n-butane with respect to the reaction time on the 0.95 wt.% of alkali (K, Ca, Na and Li) doped (PtSn)_{1.5} and the reaction was carried out at 823 K for 5 h catalysts for n-butane dehydrogenation. The initial conversion of K_{0.95}(PtSn)_{1.5}, Ca_{0.95}(PtSn)_{1.5}, Na_{0.95}(PtSn)_{1.5} and Li_{0.95}(PtSn)_{1.5} catalyst were 44.1%, 37.6%, 8.6% and 5.0%. The conversion of each catalyst after 5 h decreased to 42.8, 33.8, 7.1 and 4.9%, respectively. The conversion of the K_{0.95}(PtSn)_{1.5} catalyst was not only the highest among the prepared catalysts, but also the most stable. Both the conversion of n-butane and the stability of the catalysts were in the order of K_{0.95}(PtSn)_{1.5} > Ca_{0.95}(PtSn)_{1.5} > Na_{0.95}(PtSn)_{1.5} > Li_{0.95}(PtSn)_{1.5}.

The deactivation parameters of 0.95 wt.% of alkali (K, Ca, Na and Li) doped (PtSn)_{1.5} catalysts are shown in Table 7 ($\Delta X = 100 \times (X_i - X_f)/X_i$, where X_i is the initial and X_f is the final conversion, respectively). The Na_{0.95}(PtSn)_{1.5} catalyst showed very high deactivation rate among the other catalysts. The Li_{0.95}(PtSn)_{1.5} catalyst showed very low deactivation parameter, but the initial and final conversions were very low among the other alkali doped

Table 6

Activity and deactivation parameter of $K_{0.95}(PtSn)_{1.5}$ catalyst with different temperatures for *n*-butane dehydrogenation reaction at 823 K and a GHSV of 18,000 mL/g_{cat}/h.

Temperature (K)	Conversion (%)		Deactivation parameter (ΔX)	Selectivity (S_i/S_f) (%)				Yield of $n\text{-}C_4^=(Y_f)$ (%)		
	Initial (X_i)	Final (X_f)		$C_1\text{-}C_3$		$n\text{-}C_4^=$				
				1-Butene	2-Butene	1-Butene	2-Butene			
773	19.6	18.5	5.61	0.2/0.2	40.4/39.8	55.8/56.1	1.5/1.7	2.1/2.2	17.7	
823	44.1	42.8	2.95	1.6/1.5	36.1/37.1	56.4/55.8	1.6/1.3	4.3/4.3	39.8	
873	62.0	52.5	15.32	5.8/6.8	32.4/31.9	51.5/51.1	1.0/0.9	9.3/9.3	43.6	

Table 7

Activity (conversion, selectivity and yield) and deactivation parameter of $(PtSn)_{1.5}$ catalyst with different alkali metals for *n*-butane dehydrogenation reaction at 823 K and a GHSV of 18,000 mL/g_{cat}/h.

Catalyst (wt.%)	Conversion (%)		Deactivation parameter (ΔX)	Selectivity (S_i/S_f) (%)				Yield of $n\text{-}C_4^=(Y_f)$ (%)		
	Initial (X_i)	Final (X_f)		$C_1\text{-}C_3$		$n\text{-}C_4^=$				
				1-Butene	2-Butene	1-Butene	2-Butene			
$K_{0.95}(PtSn)_{1.5}$	44.1	42.8	2.95	1.6/1.5	36.1/37.1	56.4/55.8	1.6/1.3	4.3/4.3	39.8	
$Ca_{0.95}(PtSn)_{1.5}$	37.6	33.8	10.10	1.5/1.8	37.1/36.6	55.7/55.7	1.5/1.7	4.2/4.2	31.2	
$Na_{0.95}(PtSn)_{1.5}$	8.6	7.1	17.44	5.4/7.1	28.5/25.7	55.4/55.1	5.7/7.0	5.0/5.1	5.7	
$Li_{0.95}(PtSn)_{1.5}$	5.0	4.9	2.00	10.0/10.7	23.9/23.2	50.5/50.5	10.7/10.6	4.9/5.0	3.6	

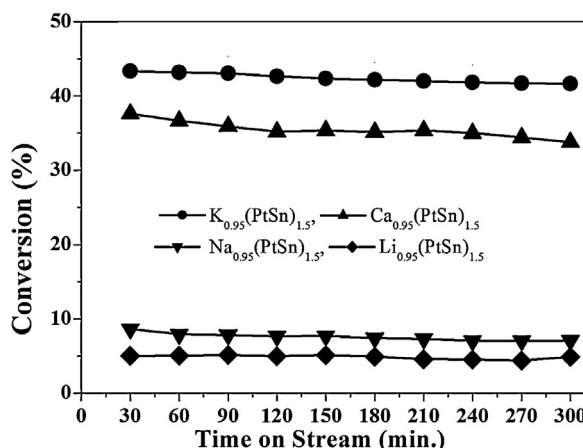


Fig. 11. Conversion vs time on stream on 0.95 wt.% alkali doped $(PtSn)_{1.5}$ catalyst for *n*-butane dehydrogenation reaction at 823 K and a GHSV of 18,000 mL/g_{cat}/h.

catalyst. The $Ca_{0.95}(PtSn)_{1.5}$ catalyst showed better $C_4^=$ yield than Na and Li doped catalyst, but this catalyst had low activity and high deactivation rate than $K_{0.95}(PtSn)_{1.5}$ catalyst. The $K_{0.95}(PtSn)_{1.5}$ catalyst showed the best catalytic activity among the other alkali doped catalysts.

4. Conclusions

$PtSn/\theta\text{-Al}_2\text{O}_3$ catalysts with different amount of potassium (0.4, 0.7, 0.95, 1.2 and 1.45 wt.%) were prepared by an impregnation method, and their catalytic activity in *n*-butane dehydrogenation was investigated at 823 K, an atmospheric pressure and a GHSV of 18,000 mL(g_{cat} h)⁻¹. XRD patterns and TEM images showed the PtSn alloy formation after the reduction of the $(PtSn)_{1.5}$ based catalysts. It was observed by HAADF STEM and corresponding EDX mapping that the components of Sn and K were observed on the same position with Pt particles on the $\theta\text{-Al}_2\text{O}_3$ support after the H₂ reduction, indicating that both Sn and K modified the characters of Pt particles. The particle sizes from the Pt dispersion by CO chemisorption were consistent with those by TEM analysis. It can be concluded from the activity test of the prepared catalysts that the conversion of *n*-butane was mostly related to the Pt disper-

sion. It has been known that the coke formed on the cracking and isomerization sites of the Pt catalysts. The formation of $C_1\text{-}C_3$ can be produced on the cracking sites, while that of i-C₄ can be done on the isomerization sites. $K_{0.9}(Pt)_{1.5}$ catalyst showed the $C_1\text{-}C_3$ selectivity of 6.5%, the i-C₄ selectivity of 5.4% and the coke amount of 2.9 wt.%. The Sn added $(PtSn)_{1.5}$ catalyst showed the low $C_1\text{-}C_3$ selectivity (1.7%) and coke amount (0.8 wt%), but the high i-C₄ selectivity (18.3%), resulting in the low $n\text{-}C_4^=$ selectivity (76.7%). When potassium was added to the $(PtSn)_{1.5}$ catalyst upto 0.95 wt.%, both the i-C₄ selectivity and the coke amount were minimized to be 1.5%–1.6% and 0.5%–0.3 wt.%, respectively. The further potassium addition rather increased the $C_1\text{-}C_3$ selectivity, the i-C₄ selectivity and the coke amount. From these experimental results, Sn addition suppressed the cracking sites on the Pt catalysts, while potassium addition blocked the isomerization sites (acid sites) on the Pt catalysts. A lot of potassium addition to the $(PtSn)_{1.5}$ rather weakened the interactions among Pt, Sn and K, resulting in the increase of the $C_1\text{-}C_3$ selectivity as well as of the i-C₄ selectivity, resulting in the highest coke amount.

Other alkali metals such as Ca, Na, and Li were tested for blocking the acid sites on the $(PtSn)_{1.5}$ catalysts in *n*-butane dehydrogenation. The potassium added catalyst was still the best one, because the potassium strongly suppressed the acidic sites as compared with other alkali metals as shown in NH₃-TPD studies. From these experimental results, the $K_{0.95}(PtSn)_{1.5}$ not only showed the highest $n\text{-}C_4^=$ yield in *n*-butane dehydrogenation, but also the highest stability.

Acknowledgements

This work was supported by the basic research project of KIST and by Converging Research Center Program through the National Research Foundation of Korea (NRF) funded by the Ministry of Education, Science and Technology (2011K000660).

References

- [1] S.D. Jackson, S. Rugmini, J. Catal. 251 (2007) 59–68.
- [2] S.T. Korhonen, S.M.K. Airaksinen, M.A. Bañares, A.O.I. Krause, Appl. Catal., A 333 (2007) 30–41.
- [3] S.M. Stagg, C.A. Querini, W.E. Alvarez, D.E. Resasco, J. Catal. 168 (1997) 75–94.
- [4] S.J. Miller, U.S. Patent 4 727 216, 1986.

- [5] Y. Zhang, Y. Zhou, X. Sheng, L. Wan, Y. Li, Y. Xiao, B. Yu, Z. Zeng, *Fuel Process. Technol.* 104 (2012) 23–30.
- [6] R.D. Cortright, J.A. Dumesic, *J. Catal.* 148 (1994) 771–778.
- [7] G.J. Siri, J.M. Ramallo-López, M.L. Casella, J.L.G. Fierro, F.G. Requejo, O.A. Ferretti, *Appl. Catal., A* 278 (2005) 239–249.
- [8] M. Ohta, Y. Ikeda, A. Igarashi, *Appl. Catal., A* 266 (2004) 229–233.
- [9] J. Llorca, N. Homs, J. León, J. Sales, J.L.G. Fierro, P.R. Piscina, *Appl. Catal., A* 189 (1999) 77–86.
- [10] R.D. Cortright, J.A. Dumesic, *J. Catal.* 157 (1995) 576–583.
- [11] G.J. Siri, G.R. Bertolini, M.L. Casella, O.A. Ferretti, *Mater. Lett.* 59 (2005) 2319–2324.
- [12] Y. Zhang, Y. Zhou, L. Wan, M. Xue, Y.Z. Duan, X. Liu, *J. Natur. Gas Chem.* 20 (2011) 639–646.
- [13] J.M. Hill, R.D. Cortright, J.A. Dumesic, *Appl. Catal., A* 168 (1998) 9–21.
- [14] M. Tasbihi, F. Feyzi, M.A. Amlashi, A.Z. Abdullah, A.R. Mohamed, *Fuel Process. Technol.* 88 (2007) 883–889.
- [15] D. Rodriguez, J. Sanchez, G. Arteaga, *J. Mol. Catal. A: Chem.* 228 (2005) 309–317.
- [16] M.L. Casella, G.J. Siri, G.F. Santori, O.A. Ferretti, M. Ramírez de Agudelo, *Langmuir* 13 (2000) 5639–5643.
- [17] Y. Zhang, Y. Zhou, L. Wan, M. Xue, Y.Z. Duan, X. Liu, *Fuel Process. Technol.* 92 (2011) 1632–1638.
- [18] L.H. Wan, Y.M. Zhou, Y.W. Zhang, Y.Z. Duan, X. Liu, M.W. Xue, *Ind. Eng. Chem. Res.* 50 (2011) 4280–4285.
- [19] S.A. Bocanegra, A.G. Ruiz, S.R. de Miguel, O.A. Scelza, *Appl. Catal., A* 277 (2004) 11–22.
- [20] S.A. Bocanegra, A.A. Castro, O.A. Scelza, S.R. de Miguel, *Appl. Catal., A* 333 (2007) 49–56.
- [21] S.A. Bocanegra, S.R. Miguel, I. Borbath, J.L. Margitfalvi, O.A. Scelza, *J. Mol. Catal. A: Chem.* 301 (2009) 52–60.
- [22] A.D. Ballarini, P. Zgolicz, I.M.J. Vilella, S.R. de Miguel, A.A. Castro, O.A. Scelza, *Appl. Catal., A* 381 (2010) 83–91.
- [23] A.D. Ballarini, C.G. Ricci, S.R. de Miguel, O.A. Scelza, *Catal. Today* 133–135 (2008) 28–34.
- [24] G.D. Angel, A. Bonilla, Y. Pena, J. Navarrete, J.L.G. Fierro, D.R. Acosta, *J. Catal.* 219 (2003) 63–73.
- [25] Y.W. Zhang, Y.M. Zhou, H. Liu, Y. Wang, Y. Xu, P.C. Wu, *Appl. Catal., A* 333 (2007) 202–210.
- [26] B.M. Nagaraja, C.-H. Shin, K.-D. Jung, *Appl. Catal., A* 467 (2013) 211–223.
- [27] S. Zhang, Y. Zhou, Y. Zhang, L. Huang, *Catal. Lett.* 135 (2010) 76–82.
- [28] O.A. Bariás, A. Holmen, E.A. Blekkan, *Catal. Today* 24 (1995) 361–364.
- [29] F.M. Dautzenberg, H.B.M. Wolters, *J. Catal.* 51 (1978) 26–39.
- [30] G. Lietz, H. Lieske, H. Spindler, W. Hanke, J. Völter, *J. Catal.* 81 (1983) 17–25.
- [31] D.L. Hoang, S.A.-F. Farrage, J. Radnik, M.-M. Pohl, M. Schneider, H. Lieske, A. Martin, *Appl. Catal., A* 333 (2007) 67–77.
- [32] R. Burch, *J. Catal.* 71 (1981) 348–359.
- [33] Y. Perak, F. Ribeiro, G. Somorjai, *J. Catal.* 178 (1998) 66–75.
- [34] J. Freil, *J. Catal.* 25 (1972) 149–160.
- [35] H.L. Gruber, *J. Phys. Chem.* 66 (1962) 48–54.
- [36] E. Garbowksi, J.-P. Candy, M. Primet, *J. Chem. Soc. Faraday Trans. I* 79 (1983) 835–844.
- [37] P.-M. Bernard, M. Primet, *J. Chem. Faraday Trans.* 86 (3) (1990) 567–570.
- [38] P.G. Menon, R.P. De Pauw, G.F. Froment, *Ind. Eng. Chem. Prod. Res. Dev.* 18 (2) (1979) 110–116.
- [39] S. Veldurthi, C.H. Shin, O.S. Joo, K.D. Jung, *Catal. Today* 185 (2012) 88–93.
- [40] E. Merlen, P. Beccat, J.C. Bertolini, P. Delichère, N. Zanier, B. Didillon, *J. Catal.* 159 (1996) 178–188.
- [41] F.M. Brinkmeyer, D.F. Rohr, U.S. Patent 4 866 211, 1987.
- [42] T. Imai, C.W. Hung, U.S. Patent 4 430 517, 1983.